RSC Advances

PAPER

View Article Online
View Journal | View Issue



Cite this: *RSC Adv.*, 2024, **14**, 19490

# The phototoxic effect of a gold-antibody-based nanocarrier of phthalocyanine on melanoma monolayers and tumour spheroids†

Nkune Williams Nkune and Heidi Abrahamse *

In recent years, photodynamic therapy (PDT) has garnered significant attention in cancer treatment due to its increased potency and non-invasiveness compared to conventional therapies. Active-targeted delivery of photosensitizers (PSs) is a mainstay strategy to significantly reduce its off-target toxicity and enhance its phototoxic efficacy. The anti-melanoma inhibitory activity (MIA) antibody is a targeting biomolecule that can be integrated into a nanocarrier system to actively target melanoma cells due to its specific binding to MIA antigens that are highly expressed on the surface of melanoma cells. Gold nanoparticles (AuNPs) are excellent nanocarriers due to their ability to encapsulate a variety of therapeutics, such as PSs, and their ability to bind with targeting moieties for improved bioavailability in cancer cells. Hence, we designed a nanobioconjugate (NBC) composed of zinc phthalocyanine tetrasulfonic acid ($ZnPcS_4$), AuNPs and anti-MIA Ab to improve $ZnPcS_4$ bioavailability and phototoxicity in two and three-dimensional tumour models. In summary, we demonstrated that this nanobioconjugate showed significant inhibitory effects on both melanoma models due to increased ROS yields and bioavailability of the melanoma cells compared to free $ZnPcS_4$.

Received 25th May 2024
Accepted 11th June 2024

DOI: 10.1039/d4ra03858d

rsc.li/rsc-advances



## 1 Introduction

Melanoma is considered a highly aggressive skin malignancy that originates from melanocytes, and its progression is challenging to predict.[1] Although melanoma is accountable for only 2% of all skin cancer diagnoses, it is responsible for 80% of dermatologic-related cancer mortalities.[2] Melanoma is asymptomatic in the early stages and is typically detected in the late stages when the metastatic spread has occurred.[3] At this stage, current therapeutic approaches such as surgery, chemotherapy, radiation therapy, and biological therapy are ineffective and have undesirable side effects, so early detection is crucial to enhancing the patient's prognosis and survival rate.[4] Therefore, it is essential to further investigate therapeutic modalities that may exclusively destroy melanoma tumours with minimal off-target toxicity in order to prolong the patient's lifespan after diagnosis.

Photodynamic therapy (PDT) is novel, underexplored technique that allows for selective destruction of tumour cells relative to normal cells.[5] This technique relies on a light-activatable molecule, referred to as a photosensitizer (PS). PSs preferentially accumulate in cancerous tissues, and upon excitation with a suitable wavelength of light, they can either emit fluorescence, which can be exploited for the diagnosis of cancer, or transform tissue molecular oxygen into reactive tumoricidal species, which in turn eradicate cancer cells.[6]

Zinc phthalocyanines are second-generation PSs that are increasingly becoming popular in PDT applications. These PSs are endowed with pivotal advantages for achieving successful PDT outcomes, such as high affinity for tumour tissues and increased photosensitizing potency.[7] In addition, they exhibit relatively negligible toxicity and are versatile, allowing for numerous applications and processing techniques. Fundamentally, their strong absorption in the therapeutic window region (600–800 nm) enables deeper tissue penetration and successful treatment of more deeply rooted tumours.[8] In recent years, zinc phthalocyanine tetrasulfonate ($ZnPcS_4$) has gained more popularity than other phthalocyanine PSs due to its high-water compatibility conferred by attached sulfonate groups.[9] Despite many positive aspects of PDT, there are a series of limitations that hamper their full adaptation in the clinical setting. Both preclinical and clinical studies screening first- and second-generation PSs highlighted the need for designing improved PSs for PDT applications to accomplish desirable therapeutic outcomes.[10] Conventional PSs tend to aggregate under aqueous conditions due to their poor water solubility, which drastically hampers their photodynamic properties as well as their bioavailability in targeted tissues.[11] Furthermore, these PSs get ingested by biological barriers *in vivo* upon administration, which also interfere with their ability to

*Laser Research Centre, Faculty of Health Sciences, University of Johannesburg, P.O. Box 17011, Doornfontein 2028, South Africa. E-mail: 217078898@student.uj.ac.za; habrahamse@uj.ac.za; Tel: +27-11-559-655*

† Electronic supplementary information (ESI) available. See DOI: https://doi.org/10.1039/d4ra03858d

eradicate cancer cells.[12] Therefore, the incorporation of nanoparticles (NPs) into PDT paradigms aims to address issues such as low water solubility, poor bioavailability, off-target toxicity, short penetration depth, and PS degradation.[4,6] NPs are inherently hydrophilic and therefore augment the water compatibility of hydrophobic PSs. They have small dimensions, which not only allow them to evade biological barriers *in vivo* but also allow them to effortlessly penetrate tumour tissues *via* the enhance permeability and retention effect (EPR).[13,14] Moreover, NPs can load a considerable amount of therapeutic drugs due to their large surface area, improving their bioavailability at tumour sites.[14]

In particular, gold nanoparticles (AuNPs) have revolutionized PDT applications due to their ability to bypass biological barriers *in vivo*, ease of synthesis and functionalization, and abilities to inflict photothermal-induced tissue destruction.[15] Furthermore, AuNPs demonstrate remarkable biocompatibility, high binding affinity, and excellent chemical and physical stability.[16] Studies have proven that $ZnPcS_4$ modified with AuNPs not only exhibits augmented passive uptake in cancer cells but also generates higher triplet lifetimes of quantum ROS yields compared to bare PS.[17] However, PSs modified with AuNPs cannot aptly differentiate healthy cells from cancerous cells and, to some extent, cause unwanted off-target toxicity.[18] To alleviate this issue, PS nanocarriers are further modified with targeting moieties (antibodies, folic acid, peptides, carbohydrate, *etc.*) that correlate with receptors exclusively overexpressed by cancer cells but not normal tissues to improve their target-specificity.[10]

Recent studies by Yue *et al.* formulated a red-absorbing PS (NBS-ER) with a strong target specificity for oestrogen receptors overexpressed by breast cancers. NBS-ER showed significant cellular uptake and phototoxic effects in breast cancer cells when compared to free PS.[19] Wu and colleagues designed an active targeted nanophotosensitizer comprised of aloe-emodin (AE) PS modified with red blood cell (RBC) membrane ferritin. The synthesised AE@RBC/Fe nanocrystals not only showed prolonged *in vivo* circulation due to biomimetic surface functionalization but also demonstrated a significant anticancer effect *via* PDT/ferroptosis synergy.[20] Another recent study developed a target-specific molecule composed of ruthenium nitrosyl (RuNO) complexes functionalized with 17$\alpha$-ethinylestradiol (EE), a semisynthetic steroidal hormone aimed at serving as a molecular Trojan horse for the targeted delivery of RuNO complexes. The synthesised molecule exhibited a strong cellular uptake towards dermal fibroblasts with a remarkable 10-fold uptake when compared to free RuNO, thus suggesting the potential drug-targeting abilities of this biomimetic steroidal conjugate.[21] Studies state that Melanoma Inhibitory Activity (MIA) is an antigen closely associated with melanoma surface proteins, which makes it more realistic for targeting in order to enhance the bioavailability of anticancer agents in melanoma cells.[4,22] In light of this, the immobilisation of melanoma tumour-targeting entities, such as anti-MIA antibodies (Ab), onto the surface of ZnPcS nanocarrier platforms would ultimately improve the safety profile and the target-selectivity of these PSs, leading to better PDT therapeutic outcomes.[4,8]

The screening of photoactive compounds is typically conducted on traditional two-dimensional (2-D) culture models, which lack cell–cell interactions and an intrinsic tumour microenvironment indispensable for tumour signaling mechanisms and drug response, thereby resulting in a discrepant malignant phenotype compared to the native tumour.[23] As a result, deceptive and non-predictive data obtained from 2-D cell culture models is always at odds with *in vivo* responses, which has led to many preclinical drug candidates failing clinical trials.[24] Such concerns compelled researchers to develop more realistic cell culture models, such as the three-dimensional (3-D) multicellular tumour spheroids (MCTS). MCTS are excellent mimics of native solid tumours since they closely resemble many aspects of solid tumours, including cellular heterogeneity, diffusion-limited circulation of oxygen and nutrients, cell-to-cell signaling, growth dynamics, cellular interactions, and inherent resistance to therapeutic drugs.[25]

Chiarante and colleagues noted that the $IC_{50}$ concentration of ZnPc-mediated PDT was almost 40 times higher than that of 2-D cell monolayers.[26]

Naidoo and colleagues developed an active-targeted nanocarrier system for $ZnPcS_4$ delivery, which demonstrated a significant inhibitory effect on A375 monolayers, inducing apoptosis in 80% of the cell population *versus* PDT treatment with free $ZnPcS_4$. Naidoo and co-workers attributed this remarkable phototoxicity to the penetrative nature of AuNPs and the targeting abilities of anti-MIA Ab, which both enhanced the internalisation of $ZnPcS_4$ in A375 cells.[8] However, little is known about the phototoxic effect of this nanocarrier on more realistic models, such as MCTS, in order to reflect *in vivo* responses and so predict clinical outcomes.

This current study reports for the first time the phototoxic effect an active-targeted nanocarrier system composed of zinc phthalocyanine tetrasulfonic acid ($ZnPcS_4$) conjugated to AuNPs with melanoma-specific targeting antibodies, anti-melanoma inhibitory activity mAb (Anti-MIA), attached on their surface, in order to improve PS bioavailability and affinity for A375 melanoma monolayers and 3-D tumour spheroid models.

## 2 Materials and methods

### 2.1 Materials and methods

Accumax™ solution (A7089), gold(III) chloride trihydrate (MKCJ4933) ($HAuCl_4 \cdot 3H_2O$, ≥99.9% trace metals basis), trisodium citrate (for molecular biology, ≥99%), tannic acid (ACS reagent) (P5493), SH-PEG2k-NH2 (MKCN4326), HCl salt, EDC *N*-(3-dimethylaminopropyl)-*N*′-ethylcarbodiimide hydrochloride ≥99.0% (0.3449), sulfo-NHS (56485) were procured from Sigma Aldrich and TrypLETM Select (1×) (12563-029) was purchased from Gibco Invitrogen. Caspase 3, 8 and 9 multiplex assay kit (ab219915) were purchased from Abcam. BCA Protein Assay Kit (23225) and H2DFCDA (D339) were purchased from Thermo Fisher.

### 2.2 Synthesis of PEGylated citrate-AuNPs

To synthesise AuNPs, 1 mL of 1% $AuHCl_4 \cdot 3H_2O$ was combined with 79 mL Millipore water in a three-neck flask under a reflux system. The second solution, comprised of 0.5 mL of tannic acid 1%, 4 mL of 1% tri-sodium citrate, and 15.5 mL of Millipore water, was mixed with the first solution, after which they were stirred at 60 °C for a few minutes until a red colour emerged, indicating the successful formation of citrate-capped AuNPs. The newly formed AuNPs were preserved at 4 °C prior to utilisation. To covalently anchor SH-PEG-$NH_2$ onto AuNP surface, 1 mL of PEG (20 mg $mL^{-1}$) dissolved in PBS was combined with an equal quantity of AuNPs and subjected to continuous agitation for a few minutes to induce ligand exchange interactions. Thereafter, the mixture underwent a 2 h incubation and was centrifuged to eliminate unbound PEG. The mass of the pellet was weighed before being resuspended in PBS to estimate the concentration of AuNPs, which allowed for the potting of a standard curve reported in our previous study using concentrations ranging from 20–200 μg $mL^{-1}$.[27]

### 2.3 Functionalization of PEGylated AuNPs with $ZnPcS_4$ and anti-MIA Ab

1 mL of AuNP-SH-PEG-$NH_2$ (1 mg $mL^{-1}$) was added to an equal volume of 125 μM $ZnPcS_4$ (Santa Cruz®: sc-264509A). The mixture underwent a 24 h agitation at 1500 rpm, after which it was centrifuged at 15 200 rpm to pellet out the $ZnPcS_4$ – AuNP-SH-PEG-$NH_2$ nanoconjugate following its solubilization in 1 mL of PBS. The attachment of anti-MIA Ab on the surface of AuNPs was performed following protocols by Naidoo *et al.* (2019) whereby a total of 200 μg $mL^{-1}$ of anti-MIA Ab (Abcam: 166932) was mixed with $ZnPcS_4$-AuNP-SH-PEG-$NH_2$ following its activation using a two-step coupling of EDC and NHS chemistry to allow the formation of a stable amide bond between Ab and the AuNPs.[2] The prepared nanobioconjugate, $ZnPcS_4$-AuNP-S-PEG-$NH_2$-anti-MIA Ab, denoted NBC, was validated through various characterization techniques. Increasing concentrations of free $ZnPcS_4$ (10–60 μM) were spectrophotometrically measured at 673 nm, and a standard curve was plotted to estimate the amount of the PS bound to $ZnPcS_4$-AuNP-S-PEG-$NH_2$-anti-MIA Ab and the loading capacity. The following equations were derived from the standard curves of $ZnPcS_4$ ($Y = 0.0013x + 0.0017$), AuNPs ($Y = 0.0006x - 0.0131$) and anti-MIA Ab ($Y = 0.0155x + 0.0235$) and loading capacity was determined using the following formula:

$$\text{Loading capacity } (\%) = \frac{\text{concetration of loaded PS}}{\text{concentration of PS in feed}} \times 100.$$

### 2.4 *In vitro* two-dimensional cell culture and 3-D multicellular tumour spheroid preparation

This study used human malignant melanoma cell line A375 procured from European Collection of Authenticated Cell Cultures (ECACC no: 88113005) and fibroblast cells (ATCC® CRL-1502™). A375 cells were nurtured in Dulbecco's Modified Eagle's medium (DMEM) basal medium enriched with 10% (v/v) Foetal Bovine Serum (FBS) (10%; FBS, F9665 Sigma-Aldrich, Johannesburg, South Africa), 1% (v/v) amphotericin-β (250 μg $mL^{-1}$; A2942 Sigma-Aldrich, Johannesburg, South Africa) and 1% (v/v) penicillin–streptomycin (10 mg $mL^{-1}$; P42942 Sigma-Aldrich, Johannesburg, South Africa). The cells were maintained in the incubator at 37 °C, 5% $CO_2$, and 85% humidity. For 2-D monolayer experiments, once the cells demonstrated an 80% confluency, they were trypsinized and plated at a concentration of $2.5 \times 10^5$ cells per 1 mL of complete media in 3.5 $cm^2$ cell culture plates. For 3-D cell culture, U-shaped bottom 96-well ultra-low attachment plates were used to generate MCTSs. Briefly, A375 cells were seeded at a density of 4000 cells per well in 200 μL of complete culture media. Thereafter, cells were incubated for 4–5 days without any physical disturbance to allow spheroids of approximately 450 μm in diameter to form, which were then transferred into 3.4 cm diameter suspension dishes for PDT studies.

### 2.5 Drug release profile

Aliquots (100 μL) of NBC were diluted with PBS (900 μL) pH 5.4 and 7.4, after which the mixtures were incubated at 37 °C. Subsequently, the samples were centrifuged at 18 000 rpm for 10 min at different time intervals (from 0 to 30 h). The supernatant of each sample was collected, their concentrations were estimated spectrophotometrically at 673 nm and. The standard curve of $ZnPcS_4$ was used to determine the amount of PS release, which was plotted in line with the correlating time.

### 2.6 Cellular uptake studies

A375 monolayers were incubated with 0.85 μM bare $ZnPcS_4$, 0.85 μM $ZnPcS_4$-AuNP and 0.85 μM NBC for 4 h, while spheroids were treated 12.73 μM bare $ZnPcS_4$, 12.73 μM $ZnPcS_4$-AuNP and 12.73 μM NBC for 24 h. The cells were rinsed twice with HBSS and lysed using a 200 μL (0.1 M NaOH + 0.1% SDS) followed by continuous pipetting. Thereafter, the lysed cells were centrifuged at 10 000 rpm 10 min, and the supernatant was collected to determine the absorbance of the $ZnPcS_4$ at 673 nm using a UV-vis spectrophotometer, which estimated the concentration of the $ZnPcS_4$ using a standard curve of different known concentrations of $ZnPcS_4$. The cellular uptake in all samples was normalized to protein content.

### 2.7 $IC_{50}$ concentration optimisation and nanoconjugate-mediated photodynamic therapy assays

To determine an $IC_{50}$ concentration of $ZnPcS_4$ that could reduce cell viability by 50%, A375 monolayer were incubated for 4 h with increasing concentration of $ZnPcS_4$ (0.125–2 μM) with and without laser irradiation, whereas spheroids were incubated for 24 h with different concentrations of $ZnPcS_4$ ranging from 1–20 μM. The cells were irradiated using a 673 nm diode laser at 10 J $cm^{-2}$ fluency with a power output of 80 mW. Post PDT, the $IC_{50}$ concentrations were estimated using a sigmoidal graph based on MTT cell viability results. The obtained concentrations were used throughout the entire duration of the study in $ZnPcS_4$, $ZnPcS_4$-AuNP and NBC-mediated PDT treatments.

**2.7.1 MTT cell viability assay.** 3-[4,5-Dimethylthiazole-2yl]-2,5-diphenyl tetrazolium bromide assay (MTT) assay (Roche, 61187100) was used to assess viability of control and experimental groups. Briefly, 24 h after PDT, the culture medium of the cells was replaced with serum-free medium containing 0.5 mg $mL^{-1}$ of MTT reagent and incubated for 4 h. After 4 h, solubilization buffer was added to each plate to make a dilution of 1 : 2 and incubated for 24 h. Subsequently, the contents were transferred into the clear 96-well plate and analysed. The VICTOR Nivo® multi-mode plate reader, (PerkinElmer, HH35940080 EN) (was used to read the absorbance of the samples at 520 nm wavelength).

**2.7.2 Cellular morphology.** Morphological changes of spheroids 24 h post-treatment were visualized using an inverted light microscope (Olympus CKX41, C5060-ADUS) attached to a digital camera.

**2.7.3 Live/dead.** Various control and experimental groups of A375 monolayers and spheroids were stained with 1 μg mL−1 ethidium bromide (EtBr) and acridine orange (AO) for 5 min in PBS. Subsequently, the cells were washed three times with PBS and analysed using fluor 488 nm and EtBr 603 nm channels on a Carl Zeiss AXio Z1 fluorescence microscope.

**2.7.4 Cytotoxicity.** The CytoTox 96 non-radioactive cytotoxicity assay (Promega, PRG1780) was used to determine the degree of cytotoxicity by measuring the amount of lactate dehydrogenase (LDH) released from the compromised cell membranes of treated cells. The LDH release was measured at 490 nm using a VICTOR Nivo® multimode plate reader (PerkinElmer, HH35940080 EN), and the results were presented with respect to the positive control, which presented 100% cytotoxicity.

**2.7.5 ROS generation.** A375 monolayers and spheroids were treated with $ZnPcS_4$, $ZnPcS_4$-AuNP and NBC with and without laser irradiation were assessed for intracellular ROS levels using the fluorescence probe DCFH-DA. The DCF fluorescence in single-cell suspensions various groups of A375 monolayers and spheroids was measured using a VICTOR Nivo® multimode plate reader set at fluorescein (485 nm/535 nm) probe following protocols described by Sarbadhikary and Dube, 2017.[28] The fluorescence intensity was normalized to protein content and data were presented as a fold change in ROS levels compared to the untreated control.

**2.7.6 Flow cytometry.** Following PDT treatment, single cell suspensions various groups of A375 spheroids and monolayers were stained with the Annexin V-FITC/PI cell death detection kit (BD Scientific: BD/556570) in line with the manufacturer protocol. This assay is able to distinguish viable cells as well as different phases of cell death, such as early apoptosis, late apoptosis and necrosis. The prepared samples were run on the BD Accuri™ C6 flow cytometer.

**2.7.7 Caspase 3, 8 and 9 fluorometric assay.** 24 h after PDT treatment, prepared lysates of A375 monolayers and spheroids experimental groups were mixed with caspase solutions in a 96-well clear bottom plate and incubated for 1 h. The PerkinElmer, VICTOR Nivo™ was used to record fluorescence at the following wavelengths: Ex/Em = 535/620 nm (Caspase 3), Ex/Em = 490/525 nm (Caspase 8), Ex/Em = 370/450 nm (Caspase 9). The fluorescent intensity was measured using the relative fluorescence unit (RFU), and the results for each experimental group were plotted as a fold change in caspase activity relative to the control.

### 2.8 Statistical analysis

The results were depicted as the mean ± standard error (SE) value of 3 separate experiments. Data analysis was carried out using one-way ANOVA (Dunnett test) using SigmaPlot version 12.0 software. A $P$ value < 0.05 (*), 0.01 (**), and 0.001 (***) was considered statistically significant.

## 3 Results

### 3.1 Drug release profile

The release of $ZnPcS_4$ from AuNP-Anti-MIA Ab was measured spectrophotometrically over a 30 hour period in both pH 5.4 and 7.4 PBS buffers to replicate the pH conditions in the body and the acidic tumour environment (Fig. 1). More than 30% of $ZnPcS_4$ was released at both pHs within the initial 8 h, whereas the correlating values evaluated after a release time of 30 h were 79.3% ± 6.53 at pH = 5.4 and 58% ± 3.09 at pH = 7.4.

### 3.2 Cellular uptake studies of the nanobioconjugate in A375 monolayers and spheroids

A375 monolayers and were incubated with equal concentrations of bare ($ZnPcS_4$ 0.85 μM), $ZnPcS_4$-AuNP (0.85 μM) or NBC (0.85 μM) and incubated for 4 h. With reference to Fig. 2A, cells treated with bare $ZnPcS_4$ showed low PS absorption, as only 0.37 μM of the 0.85 μM administered $ZnPcS_4$ was retained post incubation. A noticeable difference was noted in cells treated with 0.85 μM $ZnPcS_4$-AuNP, with 0.56 μM recovered 4 h post-incubation *versus* free $ZnPcS_4$ ($P$ < 0.05*). The highest cellular uptake was exhibited by cells incubated with NBC, whereby 0.68 μM was retained post 4 h incubation when compared to free $ZnPcS_4$ ($P$ < 0.01**). Similarly, A375 spheroids were incubated with equal concentrations of bare $ZnPcS_4$ (12.73 μM), $ZnPcS_4$-AuNP (12.73 μM) or NBC (12.73 μM). We previously reported that spheroids incubated with free $ZnPcS_4$ exhibited poor PS

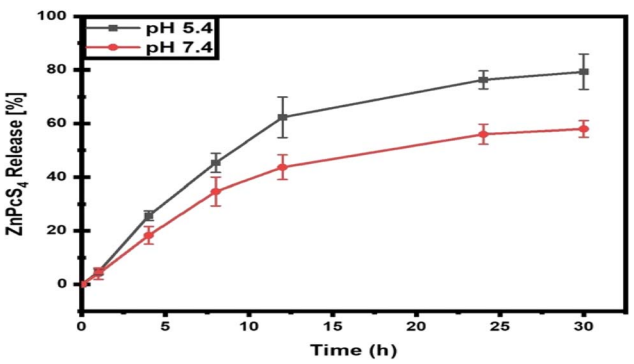


Fig. 1 $ZnPcS_4$ release kinetics from the nanoconjugate at both neutral and acidic pHs.

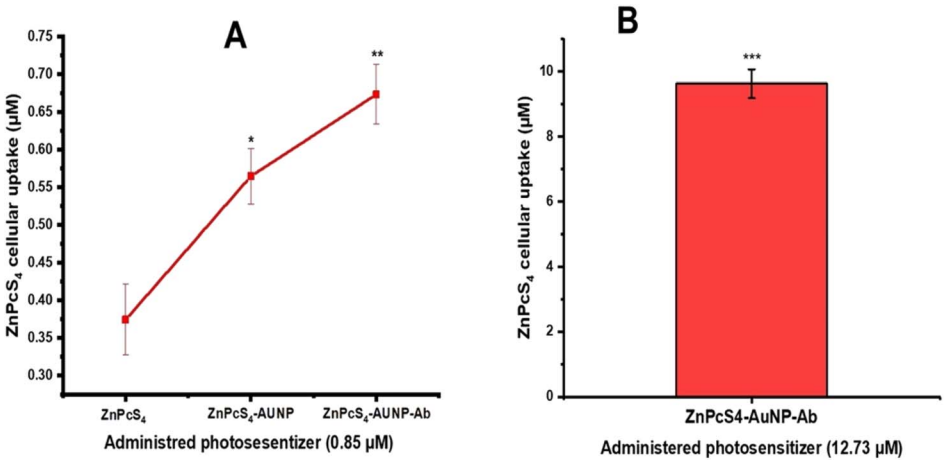


Fig. 2 Intracellular uptake of $ZnPcS_4$ in A375 monolayers and spheroids treated with a predetermined concentration of $ZnPcS_4$, 0.85 μM and 12.73 μM, respectively. (A) A375 monolayers (B) spheroids.

uptake, with roughly 4 μM of the 12.73 μM administered $ZnPcS_4$ was retained post incubation. A noticeable enhancement in cellular uptake was demonstrated by spheroids incubated with $ZnPcS_4$-AuNP treatment, with 7.4 of 12.73 μM recovered in spheroids post treatment *versus* free PS ($P < 0.01$**). In Fig. 2B, spheroids incubated with NBC showed the most favourable bioavailability revealing that 9.6 μM of the administered 12.73 μM was recovered after treatment *versus* treatment with free $ZnPcS_4$ ($P < 0.001$***).

### 3.3 Dose response studies and $IC_{50}$ concentration estimation

A375 monolayers were subjected to increasing concentrations of $ZnPcS_4$ (0.125–2 μM) and laser irradiation at a fluency of 10 J $cm^{-2}$. No inhibitory effect was detected in cells exposed to either laser irradiation or $ZnPcS_4$ alone. As observed in Fig. 3A, there was a significant dose-dependent loss in cell viability of cells treated with varying concentrations of $ZnPcS_4$. Based on the results obtained from the MTT assay, the $IC_{50}$ concentration was estimated to be 0.85 μM using a dose response curve (origins), and this concentration was used throughout the studied (Fig. 3B). We mentioned in our previous study that the $ZnPcS_4$ $IC_{50}$ concentration in A375 spheroids was 12.73 μM,[27] which was 15 times higher than in monolayers due to the resistance nature of tumour spheroids. Therefore, spheroids were treated with a dose of 12.73 μM $ZnPcS_4$ throughout the study.

### 3.4 Nanobioconjugate-mediated photodynamic therapy

#### 3.4.1 Morphology

*3.4.1.1 Monolayers.* As shown in Fig. 4, A375 monolayers controls treated with only $ZnPcS_4$, AuNPs, anti-MIA Ab, $ZnPcS_4$-AuNP and NBC (Fig. 4B–F) showed no photodamaged features when compared to untreated cells (Fig. 4A). The cells retained their distinct appearance. Likewise, cells treated with laser alone, AuNPs and anti-MIA Ab (Fig. 4G–I) combined with laser irradiation showed unaltered morphological characteristics when compared to untreated cells. However, significant alterations in morphological features were detected in PDT-treated cells with 0.85 μM $ZnPcS_4$, $ZnPcS_4$-AuNP and NBC compared

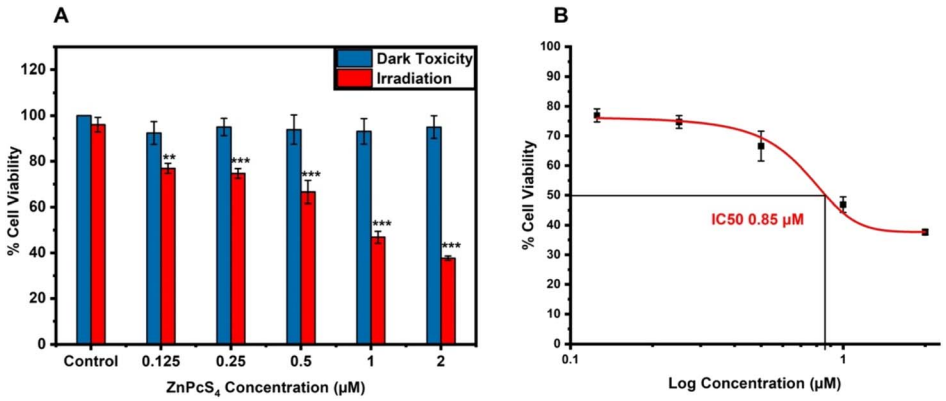


Fig. 3 (A) The response of A375 cells treated with vary concentrations of $ZnPcS_4$ (0.125–2 μM) with and without laser exposure to 673 nm laser at a fluency of 10 J $cm^{-2}$ ($P < 0.001$***). (B) A dose-response curve generated by varying concentrations of $ZnPcS_4$ (0.125–2 μM) with 673 nm laser irradiation at a fluency of 10 J $cm^{-2}$ showing an $IC_{50}$ concentration of 0.85 μM.

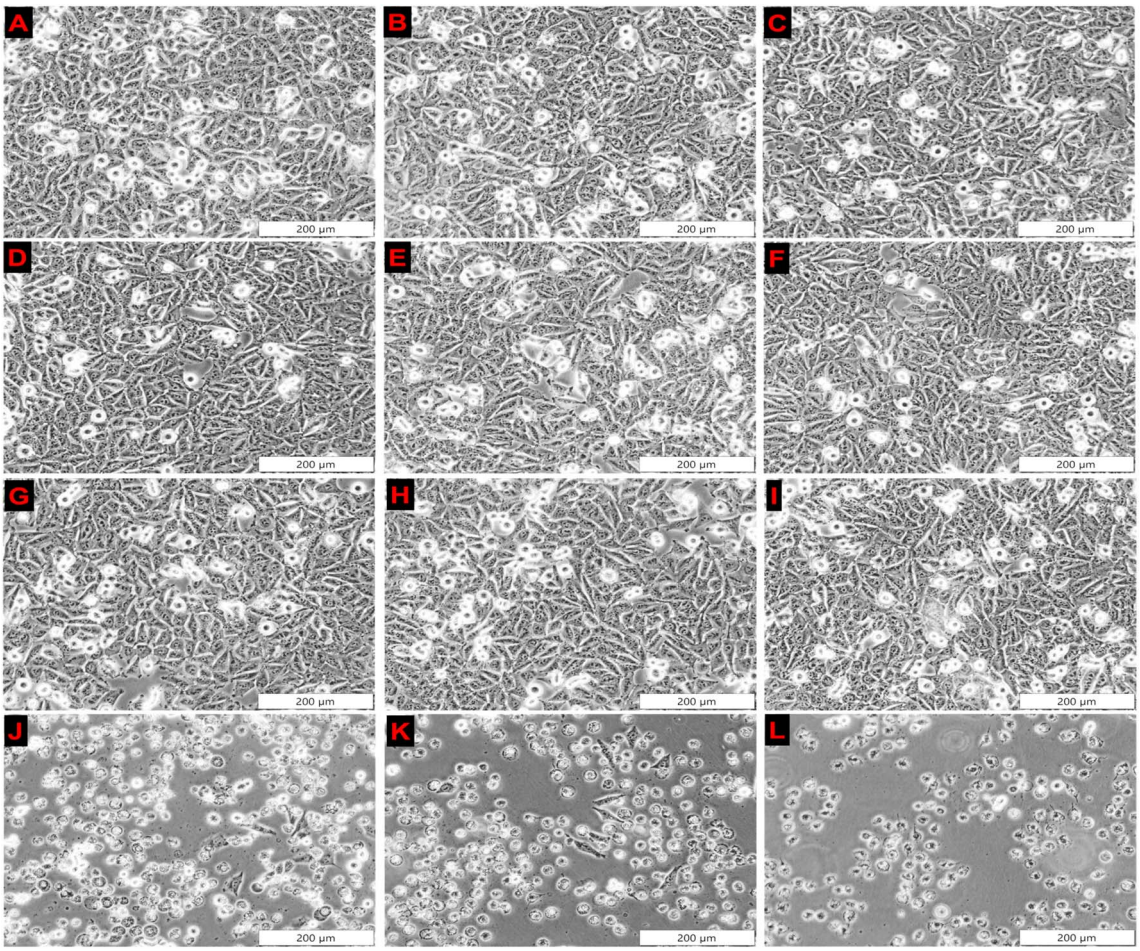


Fig. 4 Morphological assessment of spheroids following treatment with: (A) untreated spheroids, (B) $ZnPcS_4$ alone, (C) AuNP, (D) anti-MIA-Ab, (E) $ZnPcS_4$-AuNP, (F) NBC, (G) cells + irradiation, (H) AuNPs + irradiation, (I) anti-MIA-Ab + irradiation, (J) $ZnPcS_4$ + irradiation, (K) $ZnPcS_4$-AuNP and (L) NBC + irradiation.

to untreated cells (Fig. 4J–L). The cells lost their initial appearance, became round, lost their adherent properties and appeared as non-viable cell floating in culture media, indicative of cellular destruction.

*3.4.1.2 Spheroids.* In our previous study we reported that spheroids treated with free or conjugated $ZnPcS_4$ alone, laser irradiation alone, as well as irradiated and non-irradiated or AuNPs, showed no signs of photodamage when compared to untreated spheroids.[27] Similarly, spheroids treated with anti-MIA Ab with and without laser irradiation showed no altered morphology (Fig. 5A and B). Spheroids' integrity and clear outline in the periphery remained prominent. However, noticeable morphological anomalies were observed in irradiated spheroids previously incubated with free $ZnPcS_4$ and $ZnPcS_4$-AuNP.[27] In Fig. 5D, spheroids treated with NBC and laser irradiation showed significant changes in their appearance. Spheroids' outer membranes appeared disrupted, lost their distinct edge borderlines, and became encircled by debris, closely resembling photodamage in the spheroids' outer layers.

**3.4.2 Live/dead assay.** Acridine orange (AO) and ethidium bromide (EB) stains were used to determine the anticancer effects of PDT in A375 monolayers and spheroids. These stains, respectively, differentiate live and dead cells, by emitting green and red signals. As depicted in Fig. 6A–E, untreated 375 monolayers, cells exposed to laser irradiation alone and cells treated with free $ZnPcS_4$ and/or its conjugated forms exclusively emitted green fluorescence, devoid of any red fluorescent signals, suggesting no cytotoxicity. In contrast, PDT-treated groups (Fig. 6F–H) demonstrated a gradual increase in red fluorescence and attenuated green fluorescent signals, indicative of cell death. On further analysis, we noted that PDT treatment with NBC showed the highest proportion of dead cells *versus* viable ones, followed by $ZnPcS_4$-AuNP and $ZnPcS_4$. We previously showed that spheroids treated with laser irradiation alone, bare $ZnPcS_4$ alone and/or $ZnPcS_4$-AuNP exclusively showed viable cells, devoid of dead cells. Similarly, spheroids incubated with NBC (Fig. 6I) showed no phototoxicity. In contrast, we reported that PDT-treated spheroids with $ZnPcS_4$ and $ZnPcS_4$-AuNP, showed attenuated green fluorescence and an increase in red fluorescence, which suggested cytotoxicity. Similar observations were made when looking at PDT-treated spheroids with NBC, showing the most significant proportion of dead cells compared to PDT-treated groups as previously reported (Fig. 6J).

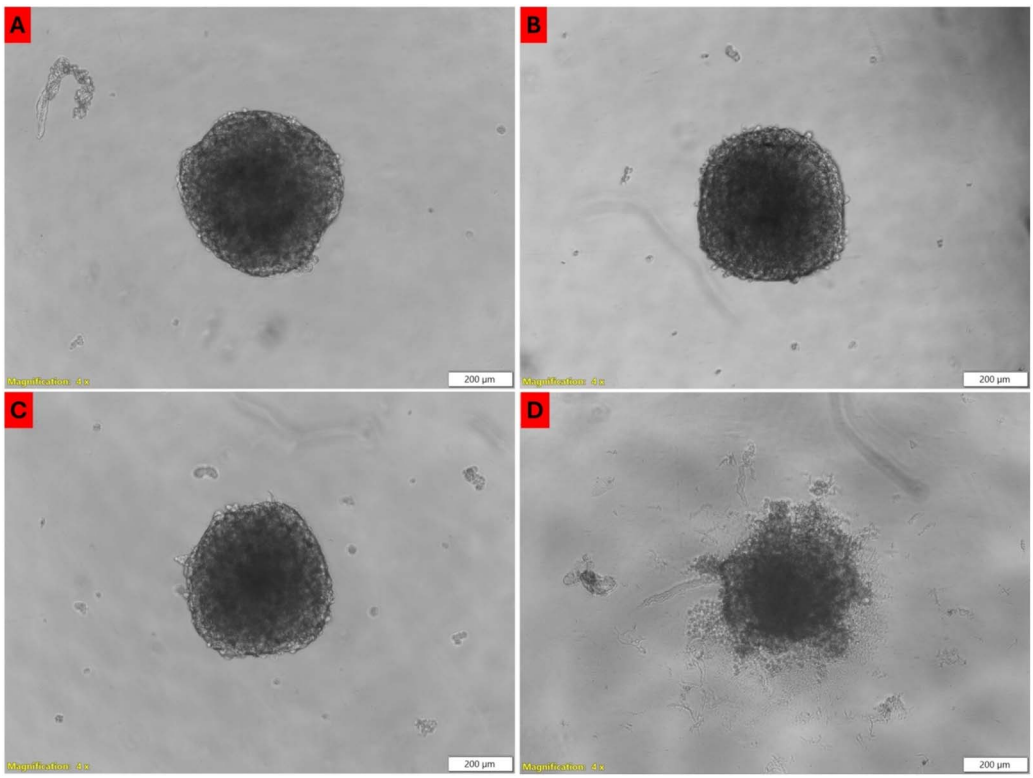


Fig. 5 Morphological assessment of spheroids following treatment with: (A) anti-MIA-Ab, (B) anti-MIA-Ab + irradiation, (C) NBC, (D) NBC + irradiation.

**3.4.3 Cytotoxicity.** As observed in Fig. 7A, LDH levels were detected in A375 monolayers to determine the extent of cell membrane disruption induced by photodamaging effects of $ZnPcS_4$. The amount of LDH release was almost undetectable in untreated cells. Likewise, cells exposed to laser irradiation alone or subjected to inactivated free $ZnPcS_4$ and/or its conjugated forms showed insignificant LDH release, suggesting negative phototoxicity. Furthermore, there was no cell membrane damage detected in cells incubated with anti-MIA Ab or AuNPs. Similarly, no detectable LDH release was observed in cells subjected to same treatments followed by photoactivation when compared to untreated control cells. However, elevated levels of LDH release were achieved in all PDT-treated cells *versus* untreated cells ($P < 0.001$***). Cells treated with 0.85 μM $ZnPcS_4$ demonstrated a 52% LDH release. Noticeably, higher levels of LDH were found in cells treated with $ZnPcS_4$-AuNP and the NBC, with a 64% and 75% increase cytotoxicity, respectively. As illustrated in Fig. 7B, the rate of LDH release in spheroids treated with free or conjugated $ZnPcS_4$ alone, laser irradiation alone, as well as with irradiated and non-irradiated anti-MIA Ab or AuNPs, was not substantially different from that of untreated spheroids, suggesting negative phototoxicity. A significant 46% increase in LDH levels was detected in spheroids subjected to $ZnPcS_4$ and laser irradiation *versus* untreated spheroids ($P <$ 0.001***). A significantly higher amount of LDH release (55%) was noted in irradiated spheroids treated with $ZnPcS_4$-AuNP, however conjugated, which verified that PS-AuNP can lead to favourable phototoxic effects ($P < 0.001$***). The most rapid LDH release was detected in spheroids subjected to NBC-mediated PDT, with a 68% increase *versus* untreated spheroids ($P < 0.001$***).

**3.4.4 ROS.** As observed in Fig. 8A, undetectable levels of intracellular ROS were exhibited by A375 monolayers alone, cells treated with bare $ZnPcS_4$ and/or its conjugated forms *versus* untreated cells. However, there was a noticeable 4.5-fold increase in the cells treated with $ZnPcS_4$ combined with laser irradiation with respect to untreated cells ($P < 0.001$***). Moreover, a significant increase in intracellular ROS levels was demonstrated by irradiated cells incubated with $ZnPcS_4$-AuNP, with a 5.2-fold increase *versus* untreated cells. On further analysis, we noted that PDT treatment with NBC showed a markedly increased intracellular ROS level of about 5.8-fold when compared to untreated cells. In Fig. 8B, insignificant intracellular ROS yields were found in spheroids exposed to laser irradiation alone, unbound $ZnPcS_4$, or compounds alone with respect to untreated spheroids (Fig. 8B). However, PDT treatment of spheroids with $ZnPcS_4$ had substantial 2.52-fold ROS yields in comparison with untreated spheroids ($P < 0.05$*). Greater effects were rendered by $ZnPcS_4$-AuNP, which showed a 3.65-fold increase in ROS yields *versus* untreated spheroids ($P$ < 0.001***). Moreover, significantly higher levels of ROS yields were exhibited by spheroids subjected to NBC, with a 3.81-fold increase relative to untreated spheroids ($P < 0.001$***).

**3.4.5 Cell death.** As depicted in Fig. 9A, untreated A375 monolayers, cells treated with laser irradiation, free $ZnPcS_4$ and/or nanoconjugates alone exhibited the highest proportion

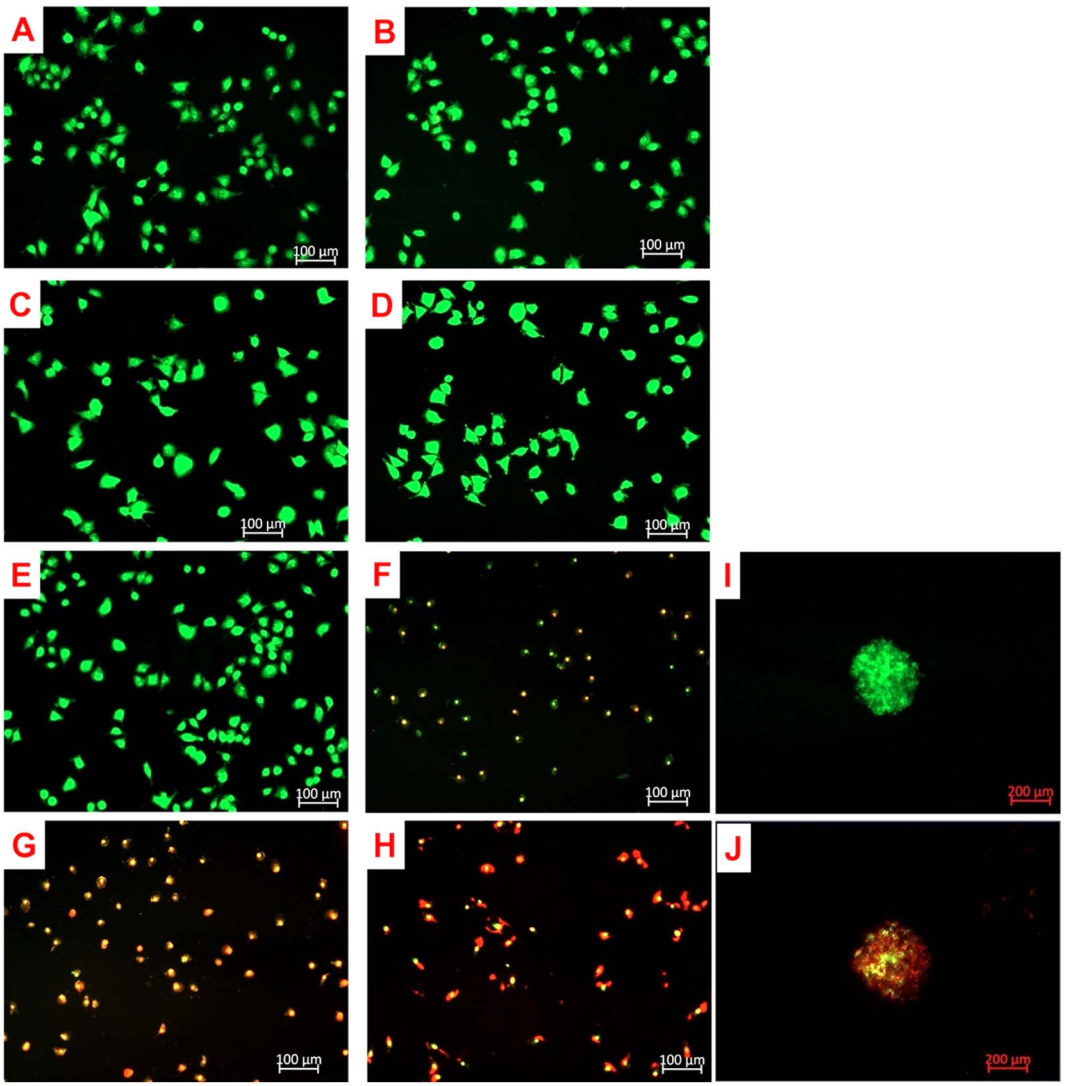


Fig. 6 Fluorescent images of acridine orange (fluor 488 nm) and ethidium bromide (603 nm) double-stained A375 monolayers. Cells only (A); cells + irradiation (B); 0.85 μM $ZnPcS_4$ (C); 0.85 μM $ZnPcS_4$-AuNP (D); 0.85 μM $ZnPcS_4$-AuNP-Ab (E); $ZnPcS_4$ + irradiation (F); $ZnPcS_4$-AuNP + irradiation (G); $ZnPcS_4$-AuNP-Ab + irradiation (H); (I) spheroid + 12.73 μM NBC; (J) spheroid + 12.73 μM NBC + irradiation.

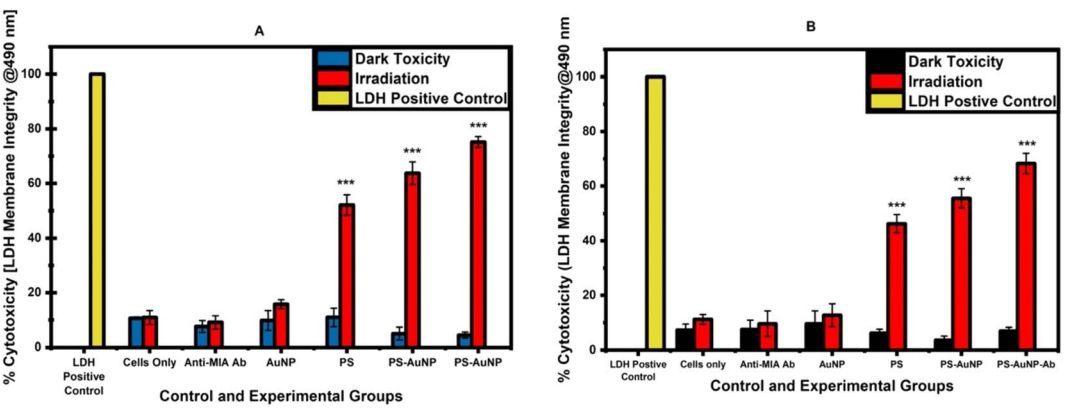


Fig. 7 The rate of LDH release in spheroids subjected to $ZnPcS_4$, $ZnPcS_4$-AuNP and NBC treatments with and without laser exposure ($P < 0.001$***). (A) A375 monolayers (B) A375 spheroids.

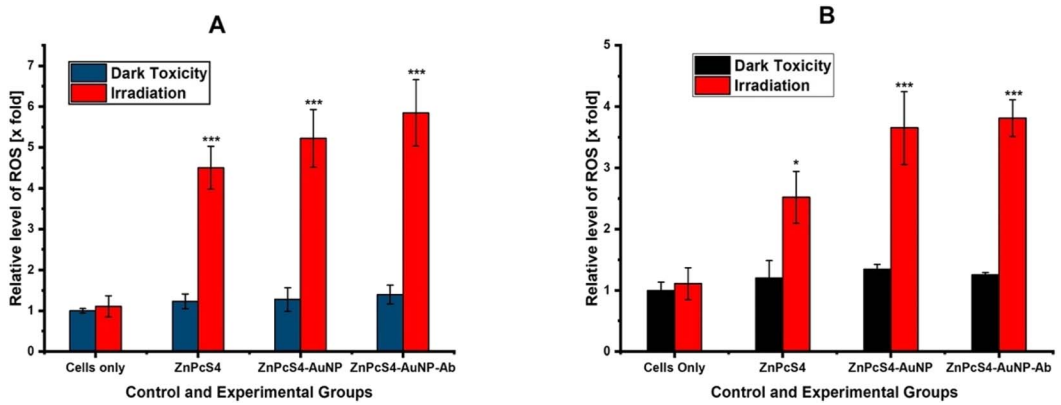


Fig. 8 Intracellular ROS yields detected in control and experiments groups of spheroids relative to untreated spheroids ($P < 0.05$* and $P < 0.001$***). (A) A375 monolayers (B) A375 spheroids.

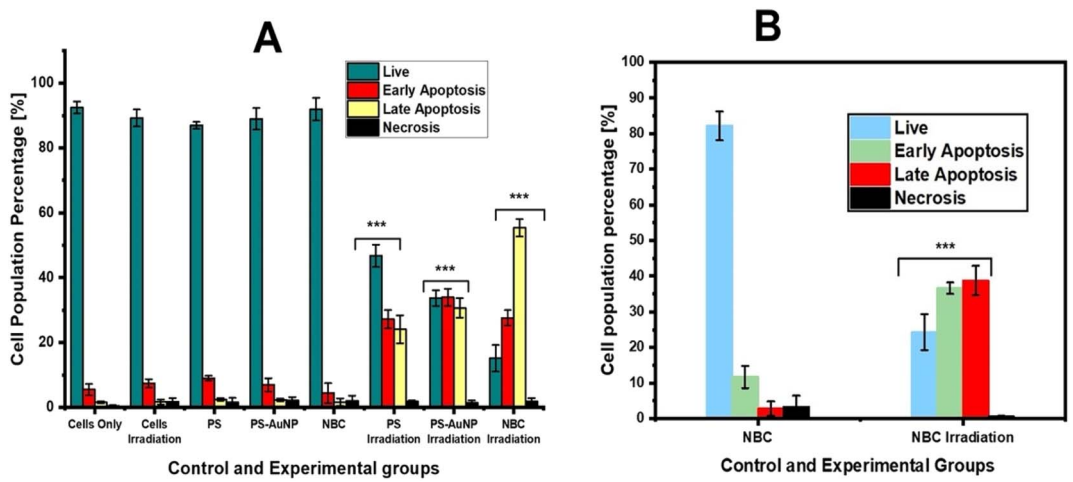


Fig. 9 The proportion of different modes of cell death induction in spheroids subjected NBC-mediated PDT treatment. (A) Monolayers (B) spheroids.

of live cells. In contrast, 0.85 μM $ZnPcS_4$ and laser irradiation caused a significant 46.7% loss in viable cell populations and resulted in 27.3% and 24.1% early and late apoptotic cell populations, respectively ($P < 0.001$***). A noticeable phototoxicity was exhibited by PDT treatment with $ZnPcS_4$-AuNP, which significantly reduced cell viability to 33.7%, while early and late apoptotic cell populations significantly increased to 33.9% and 30.7%, respectively ($P < 0.001$***). The most significant photodamaging effects was achieved by NBC-mediated PDT treatment, with a staggering 15% cell viability and increased early and late apoptotic populations to 27.6% and 55.4%, respectively ($P < 0.001$***). The most significant photodamaging effects were achieved by NBC-mediated PDT treatment, with a staggering 15% cell viability and increased early and late apoptotic populations to 27.6% and 55.4%, respectively. In our previous study we reported that irradiated spheroids alone, $ZnPcS_4$ or nanoconjugates alone revealed no evident differences in percentage cell population in contrast to untreated spheroids.[27] However, spheroids subjected to free $ZnPcS_4$ and laser irradiation showed a significant reduction in viable cell populations (47***) and increased early and late apoptotic rates (43%* and 10%, respectively). We went on to note a considerable decrease in the viable cell populations (35%**), while 42%* and 19.4%** of the cell populations were in the early and late apoptotic phases, respectively.[27] As observed in Fig. 9B, NBC-mediated PDT exhibited the most inhibitory effects by reducing the proportion of viable cells to 24.3%, with 36.6% and 38.7% increases in early and late apoptosis, respectively ($P < 0.001$***).

**3.4.6 Caspases 3, 8 and 9 expressions.** A fluorometric analysis was used to study the expression of apoptotic proteins (caspases 3, 8 and 9) in A375 monolayers and spheroids post-PDT. As observed in Fig. 10A, there was no statistical difference in the caspase activities in monolayers subjected to laser irradiation alone, free $ZnPcS_4$ and/or nanoconjugates alone *versus* untreated cells. A significant rise in caspase, 3, 8 and 9 expressions in cells treated with $ZnPcS_4$ and laser irradiation, with 2.2-fold, 2.3-fold, and 2.6-fold increases relative to untreated controls ($P < 0.001$***). A gradual increase in caspase levels was exhibited by irradiated cells previously incubated with $ZnPcS_4$-AuNP showing 2.5-fold, 2.7-fold, and 3.5-fold

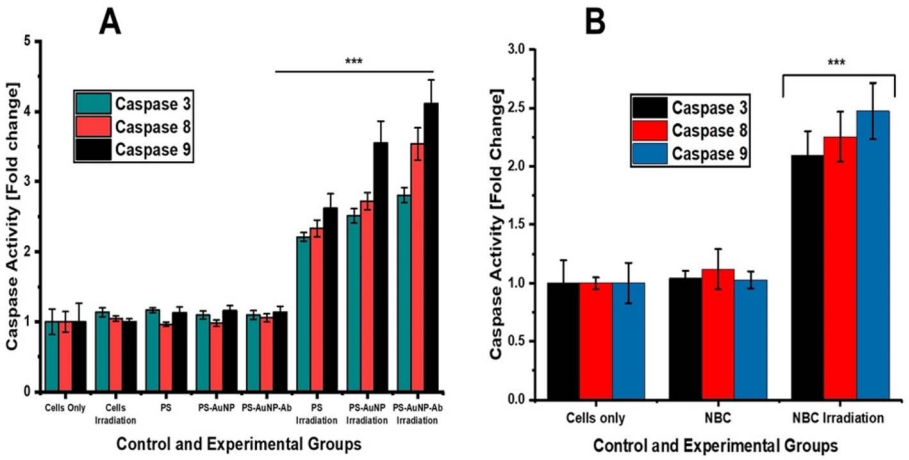


Fig. 10 Fluorometric analysis of caspase 3, 8 and 9 activities of NBC-treated A375 monolayers and spheroids. (A) Monolayers (B) spheroids.

increases in caspase 3, 8, and 9 expressions, respectively ($P <$ 0.001***). Furthermore, the most prominent rates of caspase expressions were attained by NBC-mediated PDT with 2.8-fold, 3.5-fold, and 4.1-fold increases in caspase 3, 8, and 9 activities, respectively, with respect to untreated control cells ($P <$ 0.001***). We previously reported that spheroids subjected to laser irradiation alone, free $ZnPcS_4$ and/or nanoconjugates alone exhibited no statistical difference in the caspase 3, 7 and 9 levels with respect to untreated cells. In contrast, spheroids treated with both $ZnPcS_4$ and irradiation demonstrated an increase in caspase 3, 8 and 9 with 1.6**, 1.69*** and 1.89*** folds, respectively, *versus* untreated spheroids. Furthermore, a gradual increase in caspase expressions was noted in spheroids treated with $ZnPcS_4$-AuNP and laser irradiation, showing 1.94, 1.99- and 2.27-folds increases in caspase, 3, 8 and 9, respectively, relative to untreated spheroids ($P <$ 0.001***). As observed in Fig. 10B, caspase activity was markedly increased in spheroids subjected to NBC-mediated PDT, which led to elevated levels of caspase 3, 8, and 9 by 2.1-fold, 2.25-fold, and 2.47-fold, respectively with respect to untreated control cells ($P <$ 0.001***).

## 4 Conclusion and discussion

The nanobioconjugate consisting of $ZnPcS_4$, AuNP, and anti-MIA Ab was successfully formulated and characterized (Fig. S1†). UV-vis spectral analysis proved that the NBC exhibited all the characteristic peaks of its components over a period of five weeks, suggesting photostability and conservation of PDT properties (Fig. S4†). Furthermore, there was a notable shifting and broadening of AuNP peak, suggesting an increase in molecular weight and successful chemical interactions between the components.[29] Some studies have highlighted that $ZnPcS_4$ attaches to PEGylated AuNPs through hydrogen bonding, van de Waals forces, and electrostatic interactions.[30] FTIR results of the NBC displayed distinct functional groups correlating to its constituents, as well as the existence of an amide bond between ZnPcS4-AuNP and the Ab, which was confirmed by the presence of the N–H bending at 1610–1560 (Fig. S2†).[29]

TEM revealed that the NBC had a size of 14 nm and no showed no signs of agglomeration (Fig. S3A†). As anticipated, the hydrodynamic size (215.6 nm) increased after attaching anti-MIA Ab, inferring a successful conjugation.[31] Zeta potential, however, was −19.1 mV, indicating improved stability. Studies have pointed out that negatively charged nanocarriers are remarkable delivery systems due to their ability to elude biological barriers and enhance both the passive uptake and the longevity of their cargo in circulation.[32] The current study noted a rapid release of $ZnPcS_4$ at pH 5.4 *versus* pH 7.4, concluding that the NBC could release $ZnPcS_4$ in a synchronised manner upon entering the acidic tumour environment. This is in agreement with reports by Shahidi *et al.*, who stated that AuNPs could improve the bioavailability and controlled release of drugs, thereby mitigating premature leakage of drugs in non-targeted regions.[33]

The $ZnPcS_4$ dose optimization studies yielded an $IC_{50}$ concentration of 0.85 μM in monolayers and 12.73 μM in spheroids. Studies by Gunay *et al.*, 2020 showed a 20-fold increase in the drug resistance of spheroids to PDT *versus* monolayers.[34] The reduced sensitivity of spheroids to PDT is attributed to their ability to resemble the hypoxic conditions and cellular interactions of native tumours, ultimately predicting outcomes in patients.[35]

In relation to cellular uptake studies (Fig. 6A and B), monolayers and spheroids incubated with NBC showed increased cellular uptake compared to free $ZnPcS_4$ and $ZnPcS_4$-AuNP. This is due to the fact that nanoparticles not only have a high loading capacity, but also improve the solubility and cellular uptake of PSs.[36] When further modified with targeting moieties, such as antibodies, which have a high affinity for receptors overexpressed by cancer cells, the internalisation of PS into cancer cells is increased *via* receptor-mediated endocytosis compared to free PS or non-targeted nanoconjugates.[37] These findings concurred with Studies by Sebak *et al.* which developed an active targeted nanocarrier system composed of ferrous chlorophyllin (Fe-CHL), PLGA nanoparticles, and cycloRGDyk peptide to improve PS delivery and internalisation in melanoma cells. Sebak and colleagues reported that the

nanocarrier system showed increased accumulation and singlet oxygen generation compared to free Fe-CHL, suggesting that active targeting holds great promise in cancer treatment.[38]

The phototoxic effect of NBC was revealed by morphological changes in both monolayers and spheroids. The monolayers exhibited apoptotic features such as cellular shrinkage, round shape and loss of adherent properties. These features are indicative of cellular stress, lysis and photodamage. Similar morphological changes induced by PDT were reported by Naidoo *et al.*, 2019 and Montaseri *et al.*, (2022). In addition, spheroids treated with NBC and laser irradiation showed a loss of spheroid integrity in their periphery, which suggested photodamage. Similar morphological features of damaged spheroids were reported by studies conducted by Sokolova and colleagues.[39] The outer membrane of spheroids is mostly made up of metabolically active cells, which retain significant amounts of PS and are thus more susceptible to PDT than the inner layers.[40]

The LDH release assay revealed that all controls in both monolayers and spheroids had no detrimental effects on cell membrane integrity. In monolayers, LDH release in cells treated with NBC-mediated PDT showed a significant increase in cytotoxicity of 75%, *versus* free $ZnPcS_4$ (52%) and $ZnPcS_4$-AuNP (63%) ($P < 0.001$***). Whereas in spheroids, free $ZnPcS_4$ and photoactivation led to a significant LDH release compared to the untreated control, with a 46% increase. However, a greater release was observed in irradiated spheroids previously incubated with $ZnPcS_4$-AuNP (55%). Furthermore, the most rapid LDH outburst was induced by photoactivated NBC, with a 68% increase. These findings correspond to reports by Alexeree and co-workers, who stated that AuNPs improve the solubility, cellular uptake, and optical properties of phthalocyanines, as well as their phototoxicity effect.[41] Additionally, studies have highlighted that ZnPcS PSs modified with AuNP exhibit enhanced triplet and singlet quantum yield *versus* free ZnPcS PSs.[42] Yeshchenko *et al.* attributed the significant enhancement of ROS generation of PSs combined with AuNPs to the surface plasmonic resonance of AuNPs, while the attachment of targeting moieties not only improves the bioavailability of PS molecules in cancer cells but also improves their target delivery.[43] In addition, studies have highlighted that cellular uptake mechanisms, particularly receptor-mediated endocytosis, rely on temperature.[44] In this regard, higher temperatures promote the expression of receptors on cancer cells, thereby increasing the binding affinity between the antibody and the tumour-associated antigens, ultimately increasing cellular uptake load. Inversely, lower temperatures slow down this process, potentially reducing the bioavailability of the drug.[45–47] Therefore, the incubation of the NBC at 37 °C facilitated its uptake by A375 cells.

The aforementioned statement also correlates with our ROS generation results in Fig. 8A and B, whereby conjugates of $ZnPcS_4$ PS showed improved ROS yield compared to free $ZnPcS_4$. These results correlate with studies conducted by Li *et al.*, which synthesised an active targeting nanoconjugate pyropheophorbide a (Ppa) conjugated to perfluorocarbons (PFCs) and hyaluronic acid (HA). The nanoconjugate exhibited increased ROS generation and remarkable phototoxicity *in vitro* and *in vivo in melanoma cells when compared to free Ppa*.[48] AO/dual staining in both cell culture models showed that PDT treatment with NBC the most prominent red fluorescent signals when compared to free $ZnPcS_4$ and $ZnPcS_4$-AuNP PDT treatments, which suggested an increase in late apoptotic and necrotic cells.[49] These results concur with previous studies by Ghazaeian *et al.*, 2021, which elicited same responses after PDT treatment with a nanoconjugate.[50]

Annexin-V FITC and PI flow cytometric analysis showed no obvious photodamage was induced in all control groups of monolayers and spheroids, while photoactivated NBC presented appreciable phototoxicity compared to free $ZnPcS_4$ and $ZnPcS_4$-AuNP. In monolayers, we observed a significant decrease in the proportion of viable cells (15%), as well as an increase in early and late apoptotic populations to 27.6% and 55.4%, respectively ($P < 0.001$***). These results coincided with findings by Naidoo *et al.* (2019), who noted that NBC predominately induces late apoptosis in A375 monolayers. While in spheroids, NBC reduced the ratio of viable cells to 24.3%, while 36.6% and 38.7% were cells succumbing to early and late apoptotic cell death, respectively ($P < 0.001$***). Similar outcomes were noted by Stuchinskaya and colleagues, whereby they employed an active-targeted nanocomposite to induce phototoxicity in *in vitro*-cultured cancer cells.[51] The study revealed that the AuNP-antibody-mediated phthalocyanine delivery system improved PS active intracellular accumulation and retention in tumour cells when compared to monotreatment of its constituents.

Stuchinskay and co-workers went on to report that their nanocomposite demonstrated greater apoptotic rates due to the Ab's targeting abilities and promotion of accelerated PS cellular internalisation *via* receptor-mediated endocytosis. Similar studies by Tham *et al.* synthesised a mesoporous nano-based compound composed of phthalocyanine (*Pc*), dabrafenib, and trametinib to improve cellular uptake and tumour penetration in 3-D tumour spheroids and *in vivo* tumour models. The nanocomposite showed improved phototoxicity on spheroids when compared with single treatments, resulting in 8% cell viability.[52] In addition, the nanocomposite led to 76% tumour regression *in vivo*, with no effect on non-BRAF-expressing normal cells.

Additionally, studies by Yaun *et al.* investigated the phototoxic effect of an active-targeted nanocomposite composed of chlorin e6 (Ce6) conjugated to PAMAM dendrimer (generation 7.0) functionalized with RGD peptide to enhance PS cellular uptake and tumour penetration in A375 tumour spheroids. A375 spheroids were treated with free Ce6 and the nanocomposite (800 nM) and then received a 660 nm laser at 6.3 J $cm^{-2}$. Yuan and colleagues reported that the nanocomposite significantly increased early apoptotic cells to 25.7% and 25.2% dead cells 12 h post-irradiation. On further analysis, Juan *et al.* noted that the nanocomposite exhibited 79.3-fold higher cellular uptake than free Ce6.[53] Thus, the enhanced phototoxicity effects of PDT could be attributed to the excellent accumulation and bioavailability of PS in spheroids due to the AuNPs' enhanced passive uptake and the anti-MIA Ab's high

affinity for MM cells. Several studies have proved that AuNPs induce photothermal cell destruction upon laser irradiation, whereby they convert light into lethal heat energy.[54] Studies by Rau *et al.* reported that treatment with AuNPs and 532 nm laser at 60 mW $cm^{-2}$ and 80 mW $cm^{-2}$ showed a significant inhibitory effect on the cytoskeletons of MG63 cells.[55] However, in this current study, no photodamaging effects were noted in cells treated with AuNPs and 673 nm diode laser irradiation at 10 J $cm^{-2}$ fluency with a power output of 80 mW. These findings suggest that the AuNPs could not absorb light with a 673 nm wavelength since they demonstrated a distinctive absorption peak at 520 nm. Therefore, in this study, we ruled out any possibility of AuNPs inducing photothermal cell destruction. Similar findings were reported by recent studies by Chizenga and Abrahamse, whereby AuNPs and 673 nm laser irradiation at 10 J $cm^{-2}$ fluency showed no damaging effects on cervical cells.[56]

With reference to caspase-3, -8 and -9 fluorometric analysis, we observed significantly increased caspase-3, -8, and -9 levels in both monolayers and spheroids treated with photoactivated NBC. Additionally, it was noted that caspase 9 activities were slightly higher than those of caspase 8 in all experimental groups. This clearly infers that apoptosis is not a single pathway but may integrate both mitochondrial and death receptor pathways. Similar findings were reported by,[57,58] post-treatment of skin cancer cells with chlorophyll nanoemulsion and ZnPc-PDT, respectively. In addition, studies by,[59,60] using ZnPc-mediated PDT also reported increased levels of caspase-3, 8 and 9 in skin and lung cancer cells. Overall, the results for our study suggest that the NBC induced apoptosis *via* activation of caspase cascade. In summary, active-targeted nanoparticle delivery systems hold great promise for effective PS delivery and improved therapeutic outcomes in PDT. And therefore, 3-D cell cultures are realistic models for screening anticancer agents since they closely resemble native tumours in terms of cellular interactions and drug resistance traits seen in patients.

In recent years, researchers have been actively engaged in addressing the limitations of PDT relating to anoxygenic conditions inside tumours. Studies by Ma *et al.* designed an activated targeted and oxygen self-sufficient photoactive agent composed of IR780-loaded pH-sensitive fluorocarbon-functionalized nanoparticles (SFNs) and iRGD as an active tumour targeting peptide that can penetrate deeper within the tumour.[61] Ma and colleagues reported that singlet oxygen sensor green (SOSG) revealed that the synthesised molecule showed elevated $^1O_2$ yields *in vitro* and *in vivo* upon laser irradiation (808 nm, 2 W $cm^{-2}$ for 20 s), which significantly eradicated breast cancer spheroids and *in vivo* tumours when compared to single treatments. In addition, to address the anoxygenic conditions of tumours, novel light-activated therapies that function without oxygen, such as photoactivated chemotherapy, have been investigated.

The most recent study by Bretin *et al.* developed ruthenium-mediated photoactivated chemotherapy against tumour-bearing mouse models as a new approach for treating uveal melanoma.[62] Bretin and colleagues observed that the treatment resulted in appreciable apoptotic phototoxicity and high anticancer efficacy, accompanied by rapid blood clearance and a desirable biosafety profile *in vivo*. Therefore, we warrant further research into active-targeted photoactive agents that can attenuate hypoxia or operate in an oxygen-free environment in order to achieve optimal biosafety and enhance the efficacy of cancer treatments.

## Data availability

The authors confirm that the data supporting the results are available in this article. Additional data are available from the corresponding author, upon reasonable request.

## Author contributions

N. W. N: conception and design of the study, laboratory work, acquisition of data, analysis and interpretation of data and drafting of the article. H. A: supervision of study, writing, revision of content, editing, final approval of the version to be published and corresponding author.

## Conflicts of interest

No potential conflict of interest was reported by the author(s).

## Acknowledgements

This work is based on the research supported by the South African Research Chairs Initiative of the Department of Science and Technology and National Research Foundation of South Africa (Grant no. 98337).

## References

1 Y. Liu, H. Zhao, L. Li, B. Yang, Y. Yue, M. Li, X. Shi, B. Zhang, L. Wang, C. Qi, Y. Liu, S. Ren, K. Zhang and J. Yoon, A tyrosinase-activated Pt(II) complex for melanoma photodynamic therapy and fluorescence imaging, *Sens. Actuators, B*, 2023, **374**, 132836.
2 X.-Y. Li, L.-C. Tan, L.-W. Dong, W.-Q. Zhang, X.-X. Shen, X. Lu, H. Zheng and Y.-G. Lu, Susceptibility and Resistance Mechanisms During Photodynamic Therapy of Melanoma, *Front. Oncol.*, 2020, **10**, 597.
3 N. M. Helvind, C. A. Aros Mardones, L. R. Hölmich, H. W. Hendel, P. E. Bidstrup, J. A. Sørensen and A. H. Chakera, Routine PET-CT scans provide early and accurate recurrence detection in asymptomatic stage IIB-III melanoma patients, *Eur. J. Surg. Oncol.*, 2021, **47**, 3020–3027.
4 C. Naidoo, C. A. Kruger and H. Abrahamse, Simultaneous Photodiagnosis and Photodynamic Treatment of Metastatic Melanoma, *Molecules*, 2019, **24**, 3153.
5 N. Simelane, N. W. Simelane, C. Kruger and H. Abrahamse, Photodynamic diagnosis and photodynamic therapy of colorectal cancer: in vitro and in vivo, *RSC Adv.*, 2020, **10**(68), 41560–41576.

6 N. Simelane, C. Kruger and H. Abrahamse, Targeted Nanoparticle Photodynamic Diagnosis and Therapy of Colorectal Cancer, *Int. J. Mol. Sci.*, 2021, **22**, 9779.
7 H. Montaseri, N. Nkune and H. Abrahamse, Active Targeted Photodynamic Therapeutic Effect of Silver-based Nanohybrids on Melanoma Cancer Cells, *J. Photochem. Photobiol.*, 2022, **11**, 100136.
8 C. Naidoo, C. A. Kruger and H. Abrahamse, Targeted photodynamic therapy treatment of in vitro A375 metastatic melanoma cells, *Oncotarget*, 2019, **10**, 6079–6095.
9 N. Hodgkinson, C. Kruger and H. Abrahamse, Targeted photodynamic therapy as potential treatment modality for the eradication of colon cancer and colon cancer stem cells, *Tumor Biol.*, 2017, **39**(10), DOI: **10.1177/1010428317734691**.
10 I. S. Mfouo-Tynga, L. D. Dias, N. M. Inada and C. Kurachi, Features of third generation photosensitizers used in anticancer photodynamic therapy: Review, *Photodiagn. Photodyn. Ther.*, 2021, **34**, 102091.
11 E. J. Hong, D. G. Choi and M. S. Shim, Targeted and effective photodynamic therapy for cancer using functionalized nanomaterials, *Acta Pharm. Sin. B*, 2016, **6**, 297–307.
12 C. A. Kruger and H. Abrahamse, Utilisation of Targeted Nanoparticle Photosensitiser Drug Delivery Systems for the Enhancement of Photodynamic Therapy, *Molecules*, 2018, **23**, 2628.
13 J. Wu, The Enhanced Permeability and Retention (EPR) Effect: The Significance of the Concept and Methods to Enhance Its Application, *J. Pers. Med.*, 2021, **11**, 771.
14 X. Yu, I. Trase, M. Ren, K. Duval, X. Guo and Z. Chen, Design of Nanoparticle-Based Carriers for Targeted Drug Delivery, *J. Nanomater.*, 2016, **2016**, 1087250.
15 H. Montaseri, C. Kruger and H. Abrahamse, Review: organic nanoparticle based active targeting for photodynamic therapy treatment of breast cancer cells, *Oncotarget*, 2020, **11**, 2120–2136.
16 X. Hu, Y. Zhang, T. Ding, J. Liu and H. Zhao, Multifunctional Gold Nanoparticles: A Novel Nanomaterial for Various Medical Applications and Biological Activities, *Front. Bioeng. Biotechnol.*, 2020, **8**, 990.
17 P. García Calavia, I. Chambrier, M. J. Cook, A. H. Haines, R. A. Field and D. A. Russell, Targeted photodynamic therapy of breast cancer cells using lactose-phthalocyanine functionalized gold nanoparticles, *J. Colloid Interface Sci.*, 2018, **512**, 249–259.
18 M. G. Mokwena, C. A. Kruger, M.-T. Ivan and A. Heidi, A review of nanoparticle photosensitizer drug delivery uptake systems for photodynamic treatment of lung cancer, *Photodiagn. Photodyn. Ther.*, 2018, **22**, 147–154.
19 X. Yue, T. Guo, H. Zhang, B. Wang, M. Lan and X. Song, An estradiol-functionalized red-emissive photosensitizer for enhanced and precise photodynamic therapy of breast cancers, *Chem. Commun.*, 2023, **59**, 7060–7063.
20 M. Wu, W. Ling, J. Wei, R. Liao, H. Sun, D. Li, Y. Zhao and L. Zhao, Biomimetic photosensitizer nanocrystals trigger enhanced ferroptosis for improving cancer treatment, *J. Controlled Release*, 2022, **352**, 1116–1133.
21 P. Labra-Vázquez, E. Rocha, Y. Xiao, M. Tassé, C. Duhayon, N. Farfán, R. Santillan, L. Gibot, P. G. Lacroix and I. Malfant, A Trojan horse approach for enhancing the cellular uptake of a ruthenium nitrosyl complex, *Dalton Trans.*, 2023, **52**, 18177–18193.
22 L. Ding, A. Gosh, D. J. Lee, G. Emri, W. J. Huss, P. N. Bogner and G. Paragh, Prognostic biomarkers of cutaneous melanoma, *Photodermatol., Photoimmunol. Photomed.*, 2022, **38**, 418–434.
23 B. Pinto, A. C. Henriques, P. M. A. Silva and H. Bousbaa, Three-Dimensional Spheroids as In Vitro Preclinical Models for Cancer Research, *Pharmaceutics*, 2020, **12**, E1186.
24 N. Chaicharoenaudomrung, P. Kunhorm and P. Noisa, Three-dimensional cell culture systems as an in vitro platform for cancer and stem cell modeling, *World J. Stem Cells*, 2019, **11**, 1065–1083.
25 S. Khanna, A. Chauhan, A. N. Bhatt and B. S. R. Dwarakanath, in *Animal Biotechnology*, ed. A. S. Verma and A. Singh, Academic Press, Boston, 2nd edn, 2020, pp. 251–268.
26 N. Chiarante, M. C. García Vior, J. Awruch, J. Marino and L. P. Roguin, Phototoxic action of a zinc(II) phthalocyanine encapsulated into poloxamine polymeric micelles in 2D and 3D colon carcinoma cell cultures, *J. Photochem. Photobiol., B*, 2017, **170**, 140–151.
27 N. Nkune and H. Abrahamse, The Efficacy of Zinc Phthalocyanine Nanoconjugate on Melanoma Cells Grown as Three-Dimensional Multicellular Tumour Spheroids, *Pharmaceutics*, 2023, **15**, 2264.
28 P. Sarbadhikary and A. Dube, Iodinated chlorin p6 copper complex induces anti-proliferative effect in oral cancer cells through elevation of intracellular reactive oxygen species, *Chem.-Biol. Interact.*, 2017, **277**, 137–144.
29 I. Matei, C. M. Buta, I. M. Turcu, D. Culita, C. Munteanu and G. Ionita, Formation and Stabilization of Gold Nanoparticles in Bovine Serum Albumin Solution, *Molecules*, 2019, **24**, 3395.
30 K. Siriwardana, M. Gadogbe, S. M. Ansar, E. S. Vasquez, W. E. Collier, S. Zou, K. B. Walters and D. Zhang, Ligand Adsorption and Exchange on pegylated Gold Nanoparticles, *J. Phys. Chem. C*, 2014, **118**, 11111–11119.
31 P. Khashayar, G. Amoabediny, B. Larijani, M. Hosseini and J. Vanfleteren, Fabrication and Verification of Conjugated AuNP-Antibody Nanoprobe for Sensitivity Improvement in Electrochemical Biosensors, *Sci. Rep.*, 2017, **7**(1), 16070.
32 M. J. Mitchell, M. M. Billingsley, R. M. Haley, M. E. Wechsler, N. A. Peppas and R. Langer, Engineering precision nanoparticles for drug delivery, *Nat. Rev. Drug Discovery*, 2021, **20**, 101–124.
33 M. Shahidi, O. Abazari, P. Dayati, A. Bakhshi, A. Rasti, F. Haghiralsadat, S. M. Naghib and D. Tofighi, Aptamer-functionalized chitosan-coated gold nanoparticle complex as a suitable targeted drug carrier for improved breast cancer treatment, *Nanotechnol. Rev.*, 2022, **11**, 2875–2890.
34 G. Gunay, H. A. Kirit, A. Kamatar, O. Baghdasaryan, S. Hamsici and H. Acar, The effects of size and shape of

the ovarian cancer spheroids on the drug resistance and migration, *Gynecol. Oncol.*, 2020, **159**, 563–572.

35 F. Valli, M. C. García Vior, L. P. Roguin and J. Marino, Crosstalk between oxidative stress-induced apoptotic and autophagic signaling pathways in Zn(II) phthalocyanine photodynamic therapy of melanoma, *Free Radicals Biol. Med.*, 2020, **152**, 743–754.

36 A. M. Udrea, A. Smarandache, A. Dinache, C. Mares, S. Nistorescu, S. Avram and A. Staicu, Photosensitizers-Loaded Nanocarriers for Enhancement of Photodynamic Therapy in Melanoma Treatment, *Pharmaceutics*, 2023, **15**, 2124.

37 X. Huang, N. Mu, Y. Ding, H. W. Lam, L. Yue, C. Gao, T. Chen, Z. Yuan and R. Wang, Targeted delivery and enhanced uptake of chemo-photodynamic nanomedicine for melanoma treatment, *Acta Biomater.*, 2022, **147**, 356–365.

38 A. A. Sebak, I. E. O. Gomaa, A. N. ElMeshad and M. H. AbdelKader, Targeted photodynamic-induced singlet oxygen production by peptide-conjugated biodegradable nanoparticles for treatment of skin melanoma, *Photodiagn. Photodyn. Ther.*, 2018, **23**, 181–189.

39 E. A. Sokolova, A. O. Senatskaya, S. A. Lermontova, E. K. Akinchits, L. G. Klapshina, A. A. Brilkina and I. V. Balalaeva, Model of Ovarian Adenocarcinoma Spheroids for Assessing Photodynamic Cytotoxicity, *Sovrem. Tehnol. v Med.*, 2020, **12**, 34–40.

40 S. Manoto, N. Houreld and H. Abrahamse, Resistance of Lung Cancer Cells Grown as Multicellular Tumour Spheroids to Zinc Sulfophthalocyanine Photosensitization, *Int. J. Mol. Sci.*, 2015, **16**, 10185–10200.

41 S. M. I. Alexeree, M. A. Sliem, R. M. EL-Balshy, R. M. Amin and M. A. Harith, Exploiting biosynthetic gold nanoparticles for improving the aqueous solubility of metal-free phthalocyanine as biocompatible PDT agent, *Mater. Sci. Eng., C*, 2017, **76**, 727–734.

42 E. Dube, D. Oluwole, N. Nwaji and T. Nyokong, Glycosylated zinc phthalocyanine-gold nanoparticle conjugates for photodynamic therapy: Effect of nanoparticle shape, *Spectrochim. Acta, Part A*, 2018, **203**, 85–95.

43 O. Yeshchenko, P. Khort, O. Fedotov, V. Chumachenko, P. Virych, H. S. Warren, B. W. Booth, V. Bliznyuk and N. Kutsevol, Third-Generation Anticancer Photodynamic Therapy Systems Based on Star-like Anionic Polyacrylamide Polymer, Gold Nanoparticles, and Temoporfin Photosensitizer, *Molecules*, 2024, **29**, 2224.

44 C. K. Wang, I. Nelepcu, D. Hui, H. Z. Oo, S. Truong, S. Zhao, Z. Tahiry, S. Esfandnia, F. Ghaidi, H. Adomat, R. Dagil, T. Gustavsson, S. Choudhary, A. Salanti, P. H. Sorensen, N. Al Nakouzi and M. Daugaard, Internalization and trafficking of CSPG-bound recombinant VAR2CSA lectins in cancer cells, *Sci. Rep.*, 2022, **12**, 3075.

45 S. Behzadi, V. Serpooshan, W. Tao, M. A. Hamaly, M. Y. Alkawareek, E. C. Dreaden, D. Brown, A. M. Alkilany, O. C. Farokhzad and M. Mahmoudi, Cellular Uptake of Nanoparticles: Journey Inside the Cell, *Chem. Soc. Rev.*, 2017, **46**, 4218.

46 H. D. Summers, P. Rees, M. D. Holton, M. R. Brown, S. C. Chappell, P. J. Smith and R. J. Errington, Statistical analysis of nanoparticle dosing in a dynamic cellular system, *Nat. Nanotechnol.*, 2011, **6**, 170–174.

47 S. Vranic, N. Boggetto, V. Contremoulins, S. Mornet, N. Reinhardt, F. Marano, A. Baeza-Squiban and S. Boland, Deciphering the mechanisms of cellular uptake of engineered nanoparticles by accurate evaluation of internalization using imaging flow cytometry, *Part. Fibre Toxicol.*, 2013, **10**, 2.

48 J. Li, Y. Xue, J. Tian, Z. Liu, A. Zhuang, P. Gu, H. Zhou, W. Zhang and X. Fan, Fluorinated-functionalized hyaluronic acid nanoparticles for enhanced photodynamic therapy of ocular choroidal melanoma by ameliorating hypoxia, *Carbohydr. Polym.*, 2020, **237**, 116119.

49 K. Khorsandi, R. Hosseinzadeh and E. Chamani, Molecular interaction and cellular studies on combination photodynamic therapy with rutoside for melanoma A375 cancer cells: an in vitro study, *Cancer Cell Int.*, 2020, **20**, 525.

50 M. Ghazaeian, K. Khorsandi, R. Hosseinzadeh, A. Naderi and H. Abrahamse, Curcumin-silica nanocomplex preparation, hemoglobin and DNA interaction and photocytotoxicity against melanoma cancer cells, *J. Biomol. Struct. Dyn.*, 2021, **39**, 6606–6616.

51 T. Stuchinskaya, M. Moreno, M. J. Cook, D. R. Edwards and D. A. Russell, Targeted photodynamic therapy of breast cancer cells using antibody-phthalocyanine-gold nanoparticle conjugates, *Photochem. Photobiol. Sci.*, 2011, **10**, 822–831.

52 H. P. Tham, K. Xu, W. Q. Lim, H. Chen, M. Zheng, T. G. S. Thng, S. S. Venkatraman, C. Xu and Y. Zhao, Microneedle-Assisted Topical Delivery of Photodynamically Active Mesoporous Formulation for Combination Therapy of Deep-Seated Melanoma, *ACS Nano*, 2018, **12**, 11936–11948.

53 A. Yuan, B. Yang, J. Wu, Y. Hu and X. Ming, Dendritic nanoconjugates of photosensitizer for targeted photodynamic therapy, *Acta Biomater.*, 2015, **21**, 63–73.

54 N. Manuchehrabadi and L. Zhu, in *Handbook of Thermal Science and Engineering*, ed. F. A. Kulacki, Springer International Publishing, Cham, 2017, pp. 1–33.

55 L.-R. Rau, W.-Y. Huang, J.-W. Liaw and S.-W. Tsai, Photothermal effects of laser-activated surface plasmonic gold nanoparticles on the apoptosis and osteogenesis of osteoblast-like cells, *Int. J. Nanomed.*, 2016, **11**, 3461–3473.

56 E. Chizenga and H. Abrahamse, Design and assembly of a nanoparticle, antibody, phthalocyanine scaffold for intracellular delivery of photosensitizer to human papillomavirus-transformed cancer cells, *Artif. Cells, Nanomed., Biotechnol.*, 2023, **51**, 205–216.

57 M.-H. Liu, Y.-F. Li and B.-H. Chen, Preparation of Chlorophyll Nanoemulsion from Pomelo Leaves and Its Inhibition Effect on Melanoma Cells A375, *Plants*, 2021, **10**, 1664.

58 M. A. Doustvandi, F. Mohammadnejad, B. Mansoori, H. Tajalli, A. Mohammadi, A. Mokhtarzadeh, E. Baghbani, V. Khaze, K. Hajiasgharzadeh, M. M. Moghaddam,

M. R. Hamblin and B. Baradaran, Photodynamic therapy using zinc phthalocyanine with low dose of diode laser combined with doxorubicin is a synergistic combination therapy for human SK-MEL-3 melanoma cells, *Photodiagn. Photodyn. Ther.*, 2019, **28**, 88–97.

59 A. Chota, B. P. George and H. Abrahamse, In Vitro Cell Death Mechanisms Induced by Dicoma anomala Root Extract in Combination with $ZnPcS_4$ Mediated-Photodynamic Therapy in A549 Lung Cancer Cells, *Cells*, 2022, **11**, 3288.

60 M. Doustvandi, F. Mohammadnejad and M. Mashayekhi, Investigation of caspase 9 gene expression and apoptosis induction after photodynamic therapy with zinc phthalocyanine in SW872 skin cancer cell line, *J. Adv. Med. Biomed. Res.*, 2018, **26**, 9–20.

61 S. Ma, J. Zhou, Y. Zhang, B. Yang, Y. He, C. Tian, X. Xu and Z. Gu, An Oxygen Self-sufficient Fluorinated Nanoplatform for Relieved Tumor Hypoxia and Enhanced Photodynamic Therapy of Cancers, *ACS Appl. Mater. Interfaces*, 2019, **11**, 7731–7742.

62 L. Bretin, R. Vadde, S. Zheng, S. Gerhardt, S. Zander, A. Kornienko and S. Bonnet, Testing ruthenium-based photoactivated chemotherapy on tumor-bearing mice models as a new treatment for uveal melanoma, *Photodiagn. Photodyn. Ther.*, 2023, **41**, 103403.